Thermodynamic Description of CaO-'FeO'-SiO_2 and CaO-MnO-SiO_2 Melts – a Model Approach

J. Björkvall, Du Sichen and S. Seetharaman

Division of Theoretical Metallurgy, Department of Metallurgy
Royal Institute of Technology, 100 44 Stockholm, Sweden

(Received September 8, 1998; final form December 1, 1998)

ABSTRACT

In the present work, thermodynamic calculations were carried out to obtain the oxide activities in CaO-'FeO'-SiO_2 and CaO-MnO-SiO_2 ternary homogeneous liquid silicates. Thermodynamic assessments for the CaO-SiO_2 and CaO-'FeO' systems were carried out using a slag model developed earlier in the present laboratory. Model calculations were also performed to predict the oxide activities in the ternary systems mentioned above using only the binary model parameters, which, in turn, were based on the thermodynamic information for the corresponding binary systems. Comparison between the results of model calculation and the experimental data has shown the reliability of the slag model in extrapolating and interpolating the experimental data as functions of temperature and composition in the case of both binary and ternary systems. The comparison has also shown the applicability of the model in the ternary silicate systems, where the two basic cations vary greatly in size.

1. INTRODUCTION

Thermodynamic models of molten silica containing slags can be classified into two major groups, namely structure based models and empirical or semi-empirical models. While the structure based models /1/ may provide an insight into the relationship between the thermodynamic properties and the slag structures, the lack of structural information on the silicate melts has greatly hindered any progress in this kind of approach. On the other hand, empirical or semi-empirical models based on experimental data have been more extensively used in practice. It is well known that all Si atoms are tetrahedrally bonded to four oxygen atoms in a silicate melt. As the concentration of SiO_2 increases, the SiO_4^{4-} tetrahedra start to join together, forming dimers $Si_2O_7^{6-}$, trimers $Si_3O_{10}^{8-}$, cyclic polymers and even three-dimensional networks of bridged silicate tetrahedra. The ionic two-sub-lattice model developed by Hillert *et al.* /2/ and the IRSID model developed by Gaye *et al.* /3/ are, to some extent, in line with this consideration. An alternative approach is to consider a silicate melt as a matrix of oxygen ions with different cations including Si^{4+} distributed in it. This approach was originally proposed by Lumsden /4/.

Combining the approaches of Temkin /5/, Lumsden /4/ and Hillert /2/, a thermodynamic model for ionised melts has been developed in this laboratory. The first attempt in this direction was made by Bygdén *et al.* /6/, who tried to express the activity of 'FeO' in the CaO-'FeO'-SiO_2 system. However, no attempt was made to predict the activities in the ternary using the thermodynamic data for the corresponding binary systems. The prediction was later validated by slight modification of the model /7/. Successful model predictions were made for the 'FeO'-MgO-SiO_2 and 'FeO'-MnO-SiO_2 systems using only the information of the corresponding binary systems.

It is noted that the two ternary systems studied in the previous work /7/ involve the cations, Fe^{2+}, Mg^{2+}, Mn^{2+} and Si^{4+}, of which the first three are somewhat similar in size. This would imply that the cation-O^{-2} interactions in these cases are likely to be similar. While such systems are expected to follow the theory of ideal mixing put forward by Richardson /8/, differences in cationic sizes lead to deviations from the theory due to dissimilar

cation-anion interactions. Examples of this kind of silicate systems are CaO-'FeO'-SiO_2 and CaO-'MnO'-SiO_2. The present work is an attempt to examine the applicability of the model /7/ to silicate melts containing Ca^{2+}. To enable the model descriptions of the ternary systems CaO-'FeO'-SiO_2 and CaO-MnO-SiO_2, it was found necessary to make new thermodynamic assessments of the systems CaO-SiO_2 and CaO-'FeO' and combine these with the earlier assessments of the binaries 'FeO'-SiO_2 and MnO-SiO_2.

2. MODEL DESCRIPTION

As a detailed description of the slag model has been presented in an earlier publication /7/, only a brief outline of the model is presented here to assist the readers. As mentioned earlier, a silicate melt is considered in the present approach to be an oxygen ion matrix with different cations distributed in it. Thus, a system containing m different oxides, $C1_{c1}O_{a1}$, $C2_{c2}O_{a2}$, ... $Ci_{ci}O_{ai}$, ...$Cm_{cm}O_{am}$, can be expressed as:

$$(C1^{v1}, C2^{v2}, ... Ci^{vi}, ..., Cm^{vm})_p(O^{2-})_q \quad (1)$$

where p and q are stoichiometric numbers, Ci^{vi} stands for cations, the superscript vi represents the electrical charge. The integral Gibbs energy of a solution can be expressed as:

$$G^m = \sum X_{Ci_{ci}O_{ai}} G^0_{Ci_{ci}O_{ai}} + R\,T\,p \sum y_{Ci} \ln y_{Ci} + G^E \quad (2)$$

where $X_{Ci_{ci}O_{ai}}$ and $G^0_{Ci_{ci}O_{ai}}$ represent the mole fraction and the standard Gibbs energy of oxide $Ci_{ci}O_{ai}$ respectively. y_{Ci} in eq. (2) represents the ionic fraction defined as:

$$y_{Ci} = \frac{N_{Ci}}{\sum_{j=1\ to\ m} N_{Cj}} \quad (3)$$

where N_i is the number of moles of cation Ci^{vi} and the summation covers all the cations including Si^{4+}. As a consequence of the present description that a silicate melt consists of an oxygen matrix with different cations distributed in it, a hypothetical standard state for silica where silica is completely dissociated into Si^{4+} and O^{2-} ions is used. Lumsden /4/ evaluated the energy change for the transformation of SiO_2 in network to totally dissociated Si^{4+} and O^{2-} ions based on the silica saturated liquidus in the 'FeO'-SiO_2 system. According to Lumsden /4/, the Gibbs energy change for the following reaction:

$$SiO_{s(s)} = SiO_{2(\text{totally dissociated})} \quad (4)$$

can be expressed as:

$$\Delta G = 35600 - 7.53*T \text{ (J/mol)} \quad (5)$$

G^E in equation (2) stands for the excess Gibbs energy of mixing. To encounter the interactions between different cations in the presence of oxygen ions, G^E is expressed as a function of both temperature and composition:

$$G^E = f(T, y_{Si^{4+}}) + \sum_{i=1\ to\ m-1} \left(\sum_{j=i+1\ to\ m} y_i y_j \Omega^{ij(O)} \right) \quad (6)$$

$\Omega^{ij(O)}$ in equation (6) represents the interaction between cations Ci and Cj when O^{2-} ions are present. This interaction is a function of temperature and composition:

$$\Omega^{ij(O)} = \Omega_1^{ij(O)} + \Omega_2^{ij(O)} T + \left(\Omega_3^{ij(O)} + \Omega_4^{ij(O)} T \right)(y_i - y_j) + \left(\Omega_5^{ij(O)} + \Omega_6^{ij(O)} T \right)(y_i - y_j)^2 + \ldots \quad (7)$$

The function $f(T,y_{Si^{4+}})$ in eq. (6) is to take account of the fact that when the hypothetical standard state for silica is adopted, the excess Gibbs energy is not zero as the composition approaching pure SiO_2 /7/. However, as pointed out in a previous paper /7/, this function can only be evaluated on the basis of the experimental data for compositions of very high silica contents. In view of the fact that the highest silica contents in all systems studied in this work are below 0.7 $f(T,y_{Si^{4+}})$ is arbitrarily set to zero. Further investigation based on well established experimental data is required before this function can be obtained.

According to the model, the activity of an oxide component $Ci_{ci}O_{ai}$ is related to the corresponding cation activity:

$$a_{Ci_{ci}O_{ai}} = \left(\gamma_{Ci^{vi+}} y_{Ci^{vi+}}\right)^{ci} \quad (8)$$

2.1. Assessments for Binary Systems

2.1.1. CaO-SiO_2 System

Many researchers have investigated the oxide activities in the CaO-SiO_2 melts. A number of

techniques have been employed. These include the EMF method /9-11/, mass spectrometry /12/, slag-metal equilibration technique /13/ and gas-slag equilibration technique /14-17/. The results of the different studies are not mutually consistent. This is particularly true in the case of the activity of CaO. This is illustrated in Figure 1, which is reproduced from the Slag Atlas /18/. It is seen here that the CaO activities reported by Omori and Sanbongi /11/ are one order of magnitude higher than the values suggested by Sawamura /9/ as well as Carter and Macfarlane /14/. The disagreement could be, to a great extent, due to the thermodynamic data used for the Gibbs-Duhem integration when the activities of CaO were calculated from the activities of SiO_2. However, the CaO activities reported by Sawamura /9/, Carter and Macfarlane /14/, as well as Sharma and Richardson /15/, show good agreement. While Sawamura /9/ measured the CaO activity using a double cell arrangement in his EMF measurements, Carter and Macfarlane /14/ and Sharma and Richardson /15/ evaluated the CaO activities using the equilibrium between the slag and a gas containing sulphur. In the case of silica, Kay and Taylor /16/ measured the silica activity using the equilibrium between the slag and a gas containing CO. On the other hand, Sanbongi and Omori

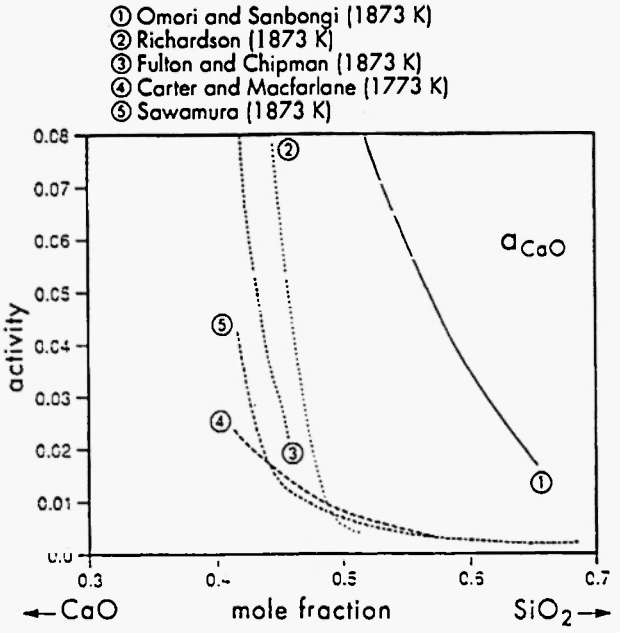

Fig. 1: Comparison of the CaO activities in the $CaO-SiO_2$ system. (Reproduced from *Slag Atlas* /18/.)

/10/ evaluated the silica activity using EMF measurement with Fe-Si alloy as the reference electrode. The results of the two investigations /10,16/ are in mutual agreement and also agree with the silica activities evaluated using Gibbs-Duhem integration from the calcium activities reported in references /9/, /14/ and /15/.

Hence, the experimental data for CaO activities from Sawamura /9/, Carter and Macfarlane /14/, and Sharma and Richardson /15/, along with the experimental points for SiO_2 activities from Sanbongi and Omori /10/ and Kay and Taylor /16/ were used in the present model calculations. The expression of optimised $\Omega^{Ca\ Si(O)}$ is presented in Table 1. The Gibbs energy of fusion for CaO is presented in Table 2. In Figure 2a, the calculated CaO activities at 1873 K are compared with the experimental values reported by Sawamura /9/, Carter and Macfarlane /14/ and Sharma and Richardson /15/. Since the CaO activity depends only slightly on temperature, the calculated activity lines for other temperatures are not included in this figure for the sake of clarity. A comparison between the calculated SiO_2 activities and the experimental data /10,16/ at 1823 K and 1903 K is presented in Figure 2b. The SiO_2 activity shows a stronger temperature dependency than the CaO activity. It is seen in both Figures 2a and 2b that the experimental data by different authors are well reproduced by the present model calculations.

2.1.2. FeO-CaO System

The FeO-CaO system in equilibrium with iron has been investigated by a number of research groups /19-23/ using different experimental techniques. Ban-Ya *et al.* /19/ employed a gas-slag equilibration technique using H_2-H_2O gas mixtures. The same technique was also used by Takeda *et al.* /20/ using CO-CO_2 gas mixture. Both Iwase *et al.* /21/ and Wijngaarden and Dippenaar /22/ carried out EMF measurements using solid electrolytes. The equilibrium between molten iron and slag was used by Fujita and Iritani /23/. In contrast to the $CaO-SiO_2$ system, the results of these investigations show excellent agreement. Hence, the results of all investigations were adopted in the model calculation. The optimised expression of $\Omega^{CaFe(O)}$ is given in Table 1. A comparison between calculated activities and experimental values is presented in Figure 3. As seen in

Table 1
Expressions for model parameters

$\Omega^{CaFe(O)}$	$-45175.2 + 10819 \cdot (y_{Ca} - y_{Fe}) + 5804.6 \cdot (y_{Ca} - y_{Fe})^2$
$\Omega^{CaMn(O)}$	$-45175.2 + 10819 \cdot (y_{Ca} - y_{Mn}) + 5804.6 \cdot (y_{Ca} - y_{Mn})^2$
$\Omega^{Ca\,Si(O)}$	$-19488.6 - 120.937 \cdot T + (-401324 + 152.341 \cdot T) \cdot (y_{Ca} - y_{Si}) - 82605.7 \cdot (y_{Ca} - y_{Si})^2$
$\Omega^{Fe\,Si(O)}$	$-28128.2 - 4627.94 \cdot (y_{Fe} - y_{Si}) + 20677.8 \cdot (y_{Fe} - y_{Si})^2$
$\Omega^{Mn\,Si(O)}$	$-104693 + 17.2827 \cdot T - 25956.7 \cdot (y_{Mn} - y_{Si}) + 27334.6 \cdot (y_{Mn} - y_{Si})^2$
$G^{E(CaFe)}_{Ca^{2+}}$	$(y_{Fe} - y_{Ca}y_{Fe}) \cdot (-45175.2 + 10819 \cdot (y_{Ca} - y_{Fe}) + 5804.6 \cdot (y_{Ca} - y_{Fe})^2) + + (y_{Ca}y_{Fe} - y_{Ca}^2 y_{Fe}) \cdot (10819 + 2 \cdot 5804.6 \cdot (y_{Ca} - y_{Fe})) - - y_{Ca}y_{Fe}^2(-10819 - 2 \cdot 5804.6 \cdot (y_{Ca} - y_{Fe}))$
$G^{E(CaFe)}_{Fe^{2+}}$	$(y_{Ca} - y_{Ca}y_{Fe}) \cdot (-45175.2 + 10819 \cdot (y_{Ca} - y_{Fe}) + 5804.6 \cdot (y_{Ca} - y_{Fe})^2) + + (y_{Ca}y_{Fe} - y_{Ca}y_{Fe}^2) \cdot (-10819 - 2 \cdot 5804.6 \cdot (y_{Ca} - y_{Fe})) - - y_{Ca}^2 y_{Fe}(10819 + 2 \cdot 5804.6 \cdot (y_{Ca} - y_{Fe}))$
$G^{E(CaMn)}_{Ca^{2+}}$	$(y_{Mn} - y_{Ca}y_{Mn}) \cdot (-45175.2 + 10819 \cdot (y_{Ca} - y_{Mn}) + 5804.6 \cdot (y_{Ca} - y_{Mn})^2) + + (y_{Ca}y_{Mn} - y_{Ca}^2 y_{Mn}) \cdot (10819 + 2 \cdot 5804.6 \cdot (y_{Ca} - y_{Mn})) - - y_{Ca}y_{Mn}^2(-10819 - 2 \cdot 5804.6 \cdot (y_{Ca} - y_{Mn}))$
$G^{E(CaMn)}_{Mn^{2+}}$	$(y_{Ca} - y_{Ca}y_{Mn}) \cdot (-45175.2 + 10819 \cdot (y_{Ca} - y_{Mn}) + 5804.6 \cdot (y_{Ca} - y_{Mn})^2) + + (y_{Ca}y_{Mn} - y_{Ca}y_{Mn}^2) \cdot (-10819 - 2 \cdot 5804.6 \cdot (y_{Ca} - y_{Mn})) - - y_{Ca}^2 y_{Mn}(10819 + 2 \cdot 5804.6 \cdot (y_{Ca} - y_{Mn}))$
$G^{E(Ca\,Si)}_{Ca^{2+}}$	$(y_{Si} - y_{Ca}y_{Si}) \cdot (-19488.6 - 120.937 \cdot T + (-401324 + 152.341 \cdot T) \cdot (y_{Ca} - y_{Si}) - 82605.7 \cdot (y_{Ca} - y_{Si})^2) + (y_{Ca}y_{Si} - y_{Ca}^2 y_{Si}) \cdot (-401324 + 152.341 \cdot T - - 82605.7 \cdot (y_{Ca} - y_{Si})^2) - y_{Ca}y_{Si}^2(401324 - 152.341 \cdot T + + 82605.7 \cdot (y_{Ca} - y_{Si})^2))$
$G^{E(Ca\,Si)}_{Si^{4+}}$	$(y_{Ca} - y_{Ca}y_{Si}) \cdot (-19488.6 - 120.937 \cdot T + (-401324 + 152.341 \cdot T) \cdot (y_{Ca} - y_{Si}) - 82605.7 \cdot (y_{Ca} - y_{Si})^2) + (y_{Ca}y_{Si} - y_{Ca}y_{Si}^2) \cdot (401324 - 152.341 \cdot T + + 82605.7 \cdot (y_{Ca} - y_{Si})^2) - y_{Ca}^2 y_{Si}(-401324 + 152.341 \cdot T - - 82605.7 \cdot (y_{Ca} - y_{Si})^2))$

Table 1 (continued)
Expressions for model parameters

$G^{E(Fe,Si)}_{Fe^{2+}}$	$(y_{Si}-y_{Fe}y_{Si})\cdot(-28128.2-4627.94\cdot(y_{Fe}-y_{Si})+20677.8\cdot(y_{Fe}-y_{Si})^2)+$ $+(y_{Fe}y_{Si}-y_{Fe}^2y_{Si})\cdot(-4627.94+2\cdot20677.8\cdot(y_{Fe}-y_{Si}))+$ $y_{Fe}y_{Si}^2(4627.94-2\cdot20677.8\cdot(y_{Fe}-y_{Si}))$
$G^{E(Fe,Si)}_{Si^{4+}}$	$(y_{Fe}-y_{Fe}y_{Si})\cdot(-28128.2-4627.94\cdot(y_{Fe}-y_{Si})+20677.8\cdot(y_{Fe}-y_{Si})^2)+$ $+(y_{Fe}y_{Si}-y_{Fe}y_{Si}^2)\cdot(4627.94-2\cdot20677.8\cdot(y_{Fe}-y_{Si}))+$ $y_{Fe}^2y_{Si}(-4627.94+2\cdot20677.8\cdot(y_{Fe}-y_{Si}))$
$G^{E(Mn,Si)}_{Mn^{2+}}$	$(y_{Si}-y_{Mn}y_{Si})\cdot(-104693+17.2827\cdot T-25956.7\cdot(y_{Mn}-y_{Si})+$ $+27334.6\cdot(y_{Mn}-y_{Si})^2+(y_{Mn}y_{Si}-y_{Mn}^2y_{Si})\cdot(-25956.7+$ $+2\cdot27334.6\cdot(y_{Mn}-y_{Si}))+y_{Mn}y_{Si}^2(25956.7-2\cdot27334.6\cdot(y_{Mn}-y_{Si}))$
$G^{E(Mn,Si)}_{Si^{4+}}$	$(y_{Mn}-y_{Mn}y_{Si})\cdot(-104693+17.2827\cdot T-25956.7\cdot(y_{Mn}-y_{Si})+$ $+27334.6\cdot(y_{Mn}-y_{Si})^2+(y_{Mn}y_{Si}-y_{Mn}y_{Si}^2)\cdot(25956.7-$ $-2\cdot27334.6\cdot(y_{Mn}-y_{Si}))+y_{Mn}^2y_{Si}(-25956.7+2\cdot27334.6\cdot(y_{Mn}-y_{Si}))$
$G^{int(Fe,Si)}_{Ca^{2+}}$	$-y_{Fe}y_{Si}(-28128.2-4627.94\cdot(y_{Fe}-y_{Si})+20677.8\cdot(y_{Fe}-y_{Si})^2)-$ $-y_{Fe}^2y_{Si}(-4627.94+2\cdot20677.8\cdot(y_{Fe}-y_{Si}))-y_{Fe}y_{Si}^2(4627.94-$ $-2\cdot20677.8\cdot(y_{Fe}-y_{Si}))$
$G^{int(Mn,Si)}_{Ca^{2+}}$	$-y_{Mn}y_{Si}(-104693+17.2827\cdot T-25956.7\cdot(y_{Mn}-y_{Si})+$ $+27334.6\cdot(y_{Mn}-y_{Si})^2)-y_{Mn}^2y_{Si}(-25956.7+27334.6\cdot(y_{Mn}-y_{Si}))-$ $-y_{Mn}y_{Si}^2(25956.7-27334.6\cdot(y_{Mn}-y_{Si}))$
$G^{int(Ca,Si)}_{Fe^{2+}}$ $G^{int(Ca,Si)}_{Mn^{2+}}$	$-y_{Ca}y_{Si}(-19488.6-120.937\cdot T+(-401324+152.341\cdot T)\cdot(y_{Ca}-y_{Si})-$ $-82605.7\cdot(y_{Ca}-y_{Si})^2)-y_{Ca}^2y_{Si}(-401324+152.341\cdot T-2\cdot82605.7\cdot$ $\cdot(y_{Ca}-y_{Si}))-y_{Ca}y_{Si}^2(401324-152.341\cdot T+2\cdot82605.7\cdot(y_{Ca}-y_{Si}))$
$G^{int(Ca,Fe)}_{Si^{4+}}$	$-y_{Ca}y_{Fe}(-45175.2+10819\cdot(y_{Ca}-y_{Fe})+5804.6\cdot(y_{Ca}-y_{Fe})^2)-$ $-y_{Ca}^2y_{Fe}(10819+5804.6\cdot(y_{Ca}-y_{Fe}))-$ $-y_{Ca}y_{Fe}^2(-10819-5804.6\cdot(y_{Ca}-y_{Fe}))$
$G^{int(Ca,Mn)}_{Si^{4+}}$	$-y_{Ca}y_{Mn}(-45175.2+10819\cdot(y_{Ca}-y_{Mn})+5804.6\cdot(y_{Ca}-y_{Mn})^2)—y_{Ca}^2y_{Mn}\cdot$ $\cdot(10819+5804.6\cdot(y_{Ca}-y_{Mn}))-y_{Ca}y_{Mn}^2(-10819-5804.6(y_{Ca}-y_{Mn}))$

Table 2
Gibbs energy of fusion

Reaction	Gibbs energy of fusion	Reference
CaO(s)=CaO(l)	$\Delta G^{\circ}_{CaO} = 79496 - 24.843 \cdot T$	32
MnO(s)=MnO(l)	$\Delta G^{\circ}_{MnO} = 43932 - 20.772 \cdot T$	32

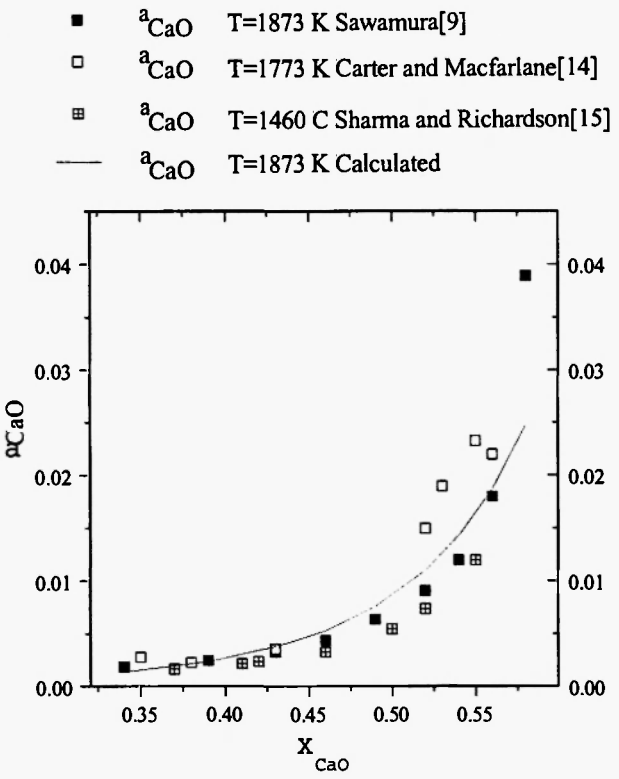

Fig. 2a: Calculated and experimentally determined /9,14,15/ activities of CaO in the CaO-SiO_2 system. The standard state is pure solid CaO.

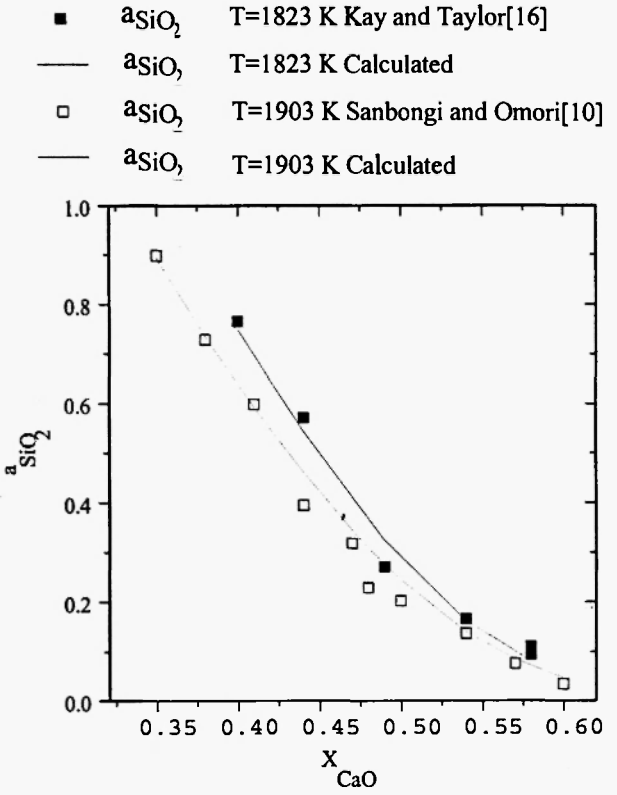

Fig. 2b: Calculated and experimentally determined /10,16/ activities of SiO_2 in the CaO-SiO_2 system. The standard state is pure solid SiO_2.

this figure, the calculated activities of 'FeO' are in very good agreement with the experimental data reported by different research groups /19-23/.

The calculated activities of CaO and 'FeO' are plotted as functions of composition for three different temperatures in Figure 4. It is seen that both the activities depend only slightly on temperature. At a given composition, the activity of CaO decreases slightly with temperature while the activity of 'FeO' shows a slight increase as the temperature increases.

2.2. Model Predictions in Ternary Systems

As mentioned earlier, one of the tasks of this work was to examine the reliability of the slag model /7/ in predicting oxide activities in the ternary systems using information only from corresponding binary systems. Hence, all the model calculations for the ternary systems were carried out using only the model parameters obtained from the binaries. While the model expressions for $\Omega^{CaSi(O)}$ and $\Omega^{CaFe(O)}$ were optimised in

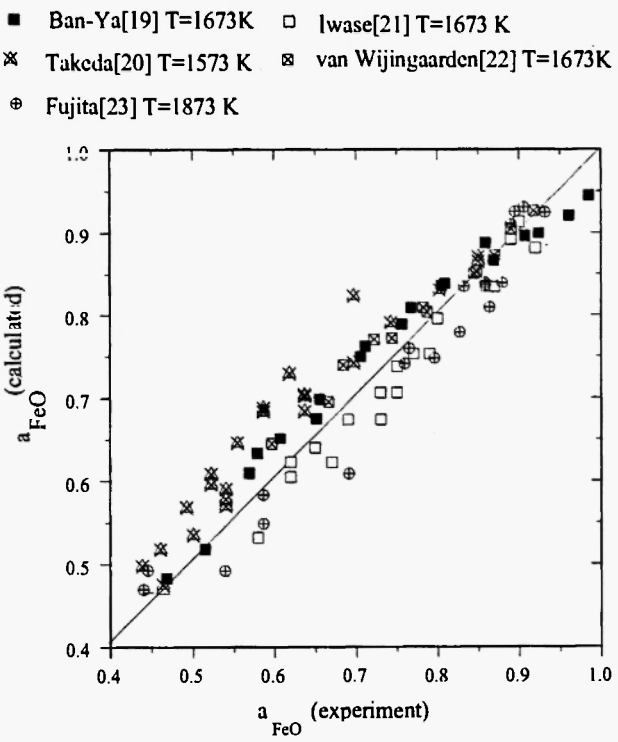

Fig. 3: Comparison between calculated activities of 'FeO'-with experimental data in the CaO-'FeO' system.

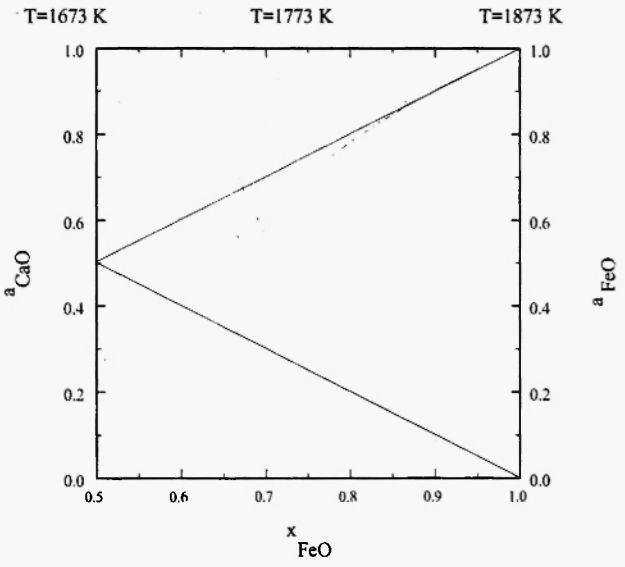

Fig. 4: Calculated activities of CaO and 'FeO' in the CaO-'FeO' system at 1673 K, 1773 K and 1873 K. The standard rates are pure liquid 'FeO' and pure solid CaO.

the present work, the equations for $\Omega^{FeSi(O)}$ and $\Omega^{MnSi(O)}$, the interactions between Fe^{2+} and Si^{4+}, as well as Mn^{2+} and Si^{4+}, in the present of oxygen ions were earlier /7/ obtained based on the experimental data in the 'FeO'-SiO_2 and MnO-SiO_2 systems, respectively.

2.2.1. *CaO-'FeO'-SiO_2*

The CaO-'FeO'-SiO_2 system in equilibrium with iron can be described as:

$$(Ca^{2+}, Fe^{2+}, Si^{4+})_p O^{2-}_q$$

The stoichiometric coefficient p is always equal to one in this system. On the other hand, the stoichiometric coefficient q will vary with composition. The possible cation interactions are between Ca^{2+} and Si^{4+}, Ca^{2+} and Fe^{2+}, and Fe^{2+} and Si^{4+} in the presence of O^{2-}. The model expressions for $\Omega^{CaSi(O)}$, $\Omega^{CaFe(O)}$ and $\Omega^{FeSi(O)}$ are available in Table 1. Using these expressions the excess Gibbs energy for the CaO-'FeO'-SiO_2 liquid phase can be expressed as:

$$G^E = y_{Ca}y_{Fe}\Omega^{CaFe(O)} + y_{Ca}y_{Si}\Omega^{CaSi(O)} + y_{Fe}y_{Si}\Omega^{FeSi(O)} \quad (9)$$

Correspondingly, the activities of CaO, 'FeO' and SiO_2 referring to their stable phases at the same temperature as standard states can be calculated by the following equations:

$$a_{CaO} = a_{Ca^{2+}}a_{O^{2-}} = a_{Ca^{2+}} = x_{CaO}\exp\left[\frac{\Delta G^0_{CaO} + G^{E(CaFe)}_{Ca^{2+}} + G^{E(CaSi)}_{Ca^{2+}} + G^{int(FeSi)}_{Ca^{2+}}}{RT}\right] \quad (10)$$

$$a_{FeO} = a_{Fe^{2+}}a_{O^{2-}} = a_{Fe^{2+}} = x_{FeO}\exp\left[\frac{\Delta G^0_{FeO} + G^{E(CaFe)}_{Fe^{2+}} + G^{E(FeSi)}_{Fe^{2+}} + G^{int(CaSi)}_{Fe^{2+}}}{RT}\right] \quad (11)$$

$$a_{SiO_2} = a_{Si^{4+}}(a_{O^{2-}})^2 = a_{Si^{4+}} = x_{SiO_2}\exp\left[\frac{\Delta G^0_{SiO_2} + G^{E(CaSi)}_{Si^{4+}} + G^{E(FeSi)}_{Si^{4+}} + G^{int(CaFe)}_{Si^{4+}}}{RT}\right] \quad (12)$$

where $a_{Ca^{2+}}$, $a_{Fe^{2+}}$ and $a_{Si^{4+}}$ represent the activities of cations Ca^{2+}, Fe^{2+} and Si^{4+} respectively, $a_{O^{2-}}$ stands for the activity of oxygen and ΔG^0_{CaO}, ΔG^0_{FeO} and $\Delta G^0_{SiO_2}$ are the Gibbs energy differences for the stan-

dard state changes of the oxides CaO, 'FeO' and SiO_2 with respect to their liquids. In eq. (10), $G^{E(CaFe)}_{Ca^{2+}}$ and $G^{E(CaSi)}_{Ca^{2+}}$ stand for the respective partial molar excess Gibbs energies of Ca^{2+} in the systems CaO-'FeO' and CaO-SiO_2 and $G^{int(FeSi)}_{Ca^{2+}}$ stands for the effect of the FeO-SiO_2 binary on the activity of Ca^{2+}. In eq. (11), $G^{E(CaFe)}_{Fe^{2+}}$ and $G^{E(FeSi)}_{Fe^{2+}}$ represent the partial excess Gibbs energies of Fe^{2+} in the binary systems CaO-'FeO' and 'FeO'-SiO_2 respectively and $G^{int(CaSi)}_{Fe^{2+}}$ stands for the effect of the CaO-SiO_2 binary on the activity of Fe^{2+}. In eq. (12), $G^{E(CaSi)}_{Si^{4+}}$ and $G^{E(FeSi)}_{Si^{4+}}$ are the partial molar excess Gibbs energies of Si^{4+} in the systems CaO-SiO_2 and FeO-SiO_2 respectively, and $G^{int(CaFe)}_{Si^{4+}}$ stands for the effect of the CaO-FeO binary on the activity of Si^{4+}. Expressions for the partial excess Gibbs energies and the effects from other binaries are given in Table 1.

Several research groups have investigated the activity of 'FeO'-in the CaO-'FeO'-SiO_2 system /24-28/. In fact, the study by Taylor and Chipman /24/ referred to in the Slag Atlas /18/ was made for complex slags containing CaO, MgO, SiO_2 and 'FeO'. When presenting their results, they added the basic oxide contents of MgO and CaO together. Bodsworth /25/ determined the 'FeO' activities using the equilibrium between a gas containing hydrogen to control the partial pressure of oxygen and the slag. Wanibe *et al.* /26/ determined 'FeO' activities in the temperature range 1523 K to 1623 K by measuring the oxygen activities in silver in equilibrium with the molten slag using a ZrO_2(CaO) solid electrolyte. Only two experimental points were presented in their paper. Timucin and Morris /27/ investigated this system at 1723 K and 1823 K. Unfortunately, no raw data was presented in their paper. Recently, Ogura *et al.* /28/ determined the 'FeO'-activity in the CaO-'FeO'-SiO_2 ternary slags using an EMF method with zirconia as solid electrolyte and Mo + MoO_2 mixture as the reference electrode. Comparison of the results /24-28/ shows that, while most of them are found to follow the same trend, the results of Bodsworth /25/ are in disagreement with the others.

The calculated iso-activity lines of 'FeO' at 1673 K are compared with the experimental data of Ogura *et al.* /28/ in Figure 5. It is seen that the experimental data are well predicted by the model calculations. Figures 6a-6c present the calculated iso-activity lines for 'FeO', CaO and SiO_2 at 1873 K, respectively.

2.2.2. CaO-MnO-SiO2

The system CaO-MnO-SiO_2 is similar to the CaO-'FeO'-SiO_2 system and may be described as:

$$(Ca^{2+}, Mn^{2+}, Si^{4+})_p O^{2-}_q$$

where the stoichiometric coefficient p is always equal to one and q is a function of composition. Three binary cation interactions in the presence of oxygen ions could be encountered, viz. those between Ca^{2+} and Si^{4+}, Ca^{2+} and Mn^{2+}, and Mn^{2+} and Si^{4+}. It is difficult to evaluate the interaction between Ca^{2+} and Mn^{2+} from the CaO-MnO binary due to the lack of experimental information. The extremely high liquidus temperatures in this system make experimental determinations very difficult. In view of the similarity of Mn^{2+} and Fe^{2+}, the expression for $\Omega^{CaFe(O)}$ was adopted for $\Omega^{CaMn(O)}$. The expressions for $\Omega^{CaSi(O)}$ and $\Omega^{MnSi(O)}$ were optimised in the present work and in an earlier study /7/, respectively. The excess Gibbs energy for the CaO-MnO-SiO_2 liquid phase can be expressed as:

$$G^E = y_{Ca} y_{Mn} \Omega^{CaMn(O)} + y_{Ca} y_{Si} \Omega^{Ca\,Si(O)} + y_{Mn} y_{Si} \Omega^{Mn\,Si(O)} \quad (13)$$

Consequently, the activities of CaO, MnO and SiO_2 with their stable phases at the same temperature as standard states are expressed as:

$$a_{CaO} = a_{Ca^{2+}} a_{O^{2-}} = a_{Ca^{2+}} = = x_{CaO} \exp\left[\frac{\Delta\tilde{G}^0_{CaO} + \tilde{G}^{E(CaMn)}_{Ca^{2+}} + \tilde{G}^{E(CaSi)}_{Ca^{2+}} + \tilde{G}^{int(MnSi)}_{Ca^{2+}}}{RT}\right] \quad (14)$$

$$a_{MnO} = a_{Mn^{2+}} a_{O^{2-}} = a_{Mn^{2+}} = = x_{MnO} \exp\left[\frac{\Delta\tilde{G}^0_{MnO} + \tilde{G}^{E(CaMn)}_{Mn^{2+}} + \tilde{G}^{E(MnSi)}_{Mn^{2+}} + \tilde{G}^{int(CaSi)}_{Mn^{2+}}}{RT}\right] \quad (15)$$

$$a_{SiO_2} = a_{Si^{4+}} (a_{O^{2-}})^2 = a_{Si^{4+}} = = x_{SiO_2} \exp\left[\frac{\Delta\tilde{G}^0_{SiO_2} + \tilde{G}^{E(CaSi)}_{Si^{4+}} + \tilde{G}^{E(MnSi)}_{Si^{4+}} + \tilde{G}^{int(CaMn)}_{Si^{4+}}}{RT}\right] \quad (16)$$

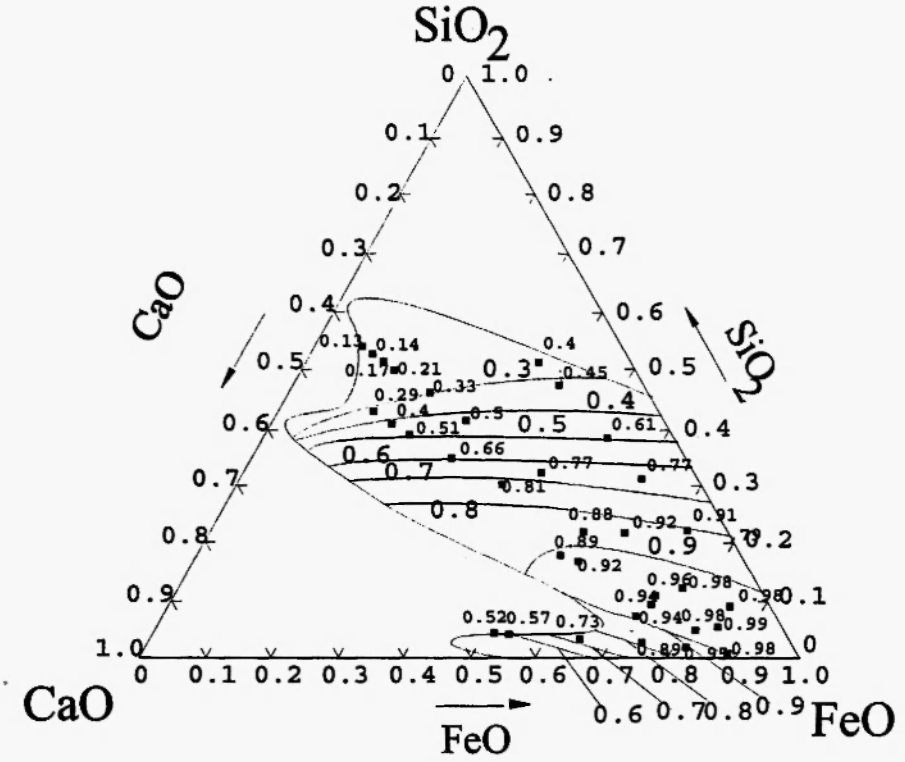

Fig. 5: Calculated and experimentally determined /28/ activities of 'FeO' in the CaO-'FeO'-SiO_2 system at 1673 K. The standard state is pure liquid 'FeO'.

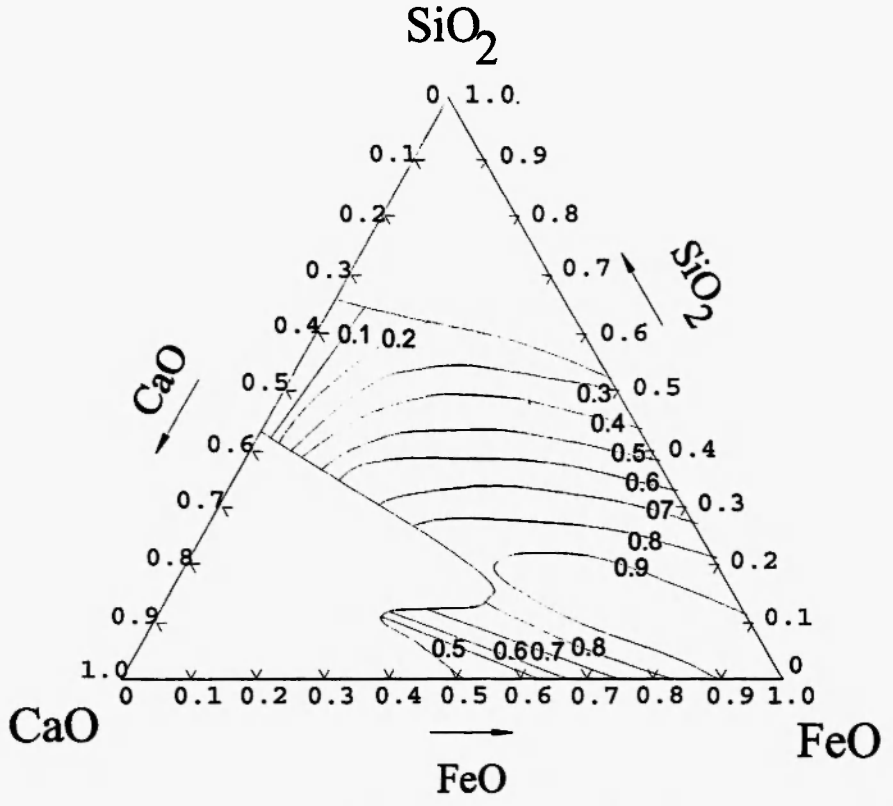

Fig. 6a: Iso activity lines of 'FeO'-in the CaO-'FeO'- SiO_2 system at 1873 K calculated by the model. The standard state is pure liquid 'FeO'.

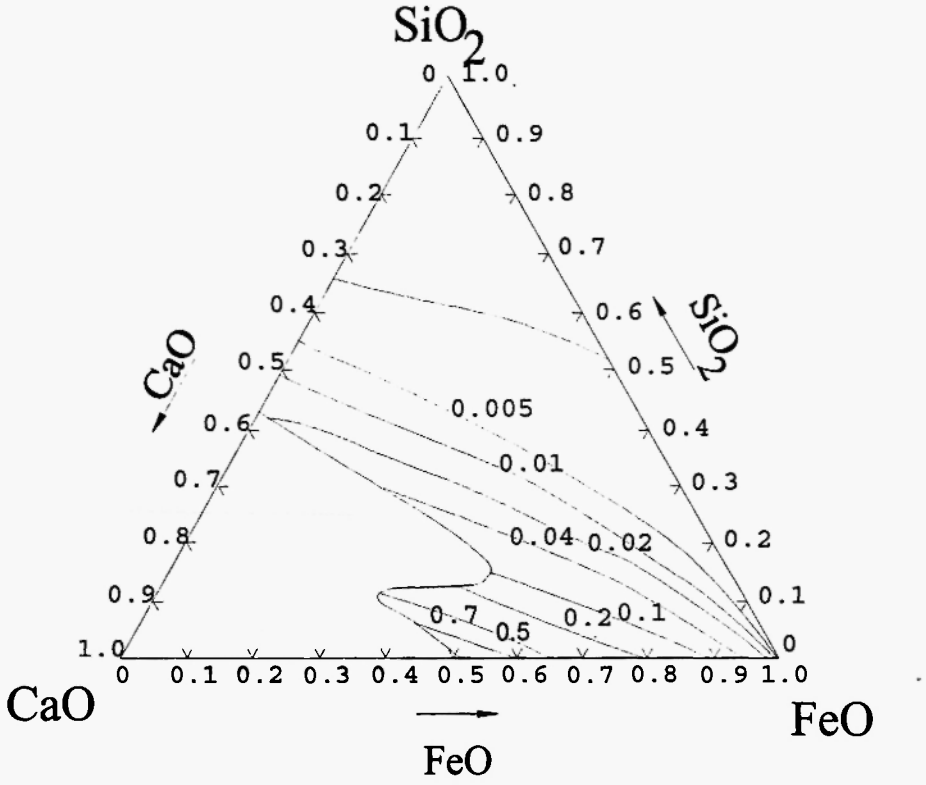

Fig. 6b: Iso activity lines of CaO in the CaO-'FeO'- SiO_2 system at 1873 K calculated by the model. The standard state is pure solid CaO.

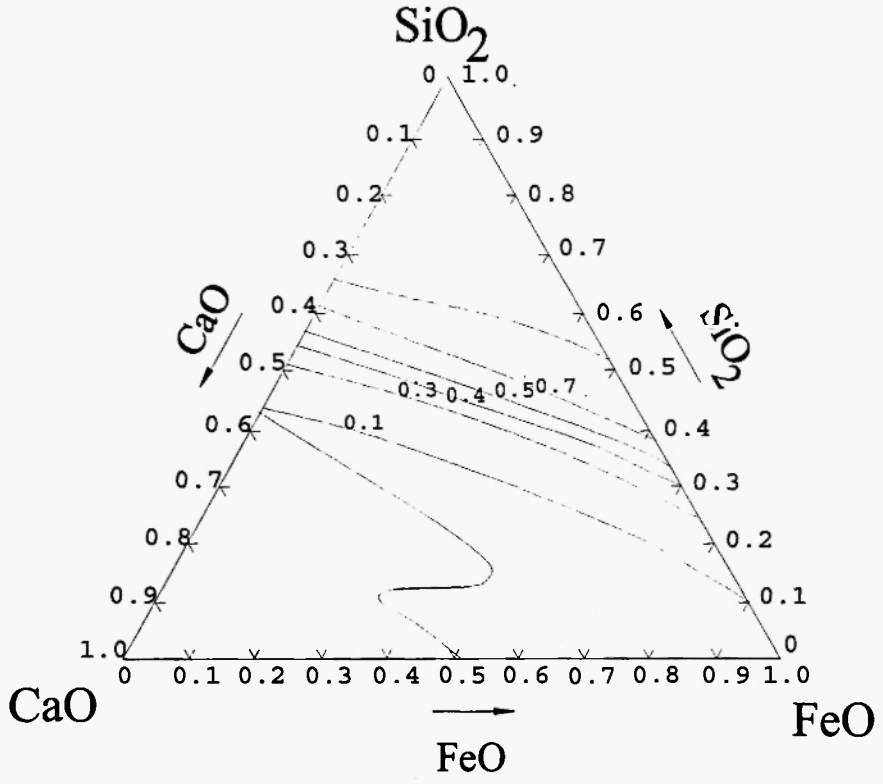

Fig. 6c: Iso activity lines of SiO_2 in the CaO-'FeO'- SiO_2 system at 1873 K calculated by the model. The standard state is pure solid SiO_2.

where $a_{Mn^{2+}}$ stands for the activity of cation Mn^{2+} and ΔG^0_{MnO} is the Gibbs energy difference for the standard state change of the oxide MnO with respect of liquid MnO. In eq. (14), $G^{E^{(CaMn)}}_{Ca^{2+}}$ represents the binary partial excess Gibbs energy of Ca^{2+} in the systems CaO- MnO and $G^{int^{(MnSi)}}_{Ca^{2+}}$, the effect of the MnO-$SiO_2$ binary on the activity of Ca^{2+}. In eq. (15), $G^{E^{(CaMn)}}_{Mn^{2+}}$ and $G^{E^{(MnSi)}}_{Mn^{2+}}$ stand for the partial excess Gibbs energies of MnO in the systems CaO-MnO and MnO-SiO_2 respectively and $G^{int^{(CaSi)}}_{Mn^{2+}}$ stands for the effect of the CaO-SiO_2 binary on the activity of Mn^{2+}. In eq. (16), $G^{E^{(MnSi)}}_{Si^{4+}}$ is the partial molar excess Gibbs energy of Si^{4+} in the system MnO-SiO_2 and $G^{int^{(CaMn)}}_{Si^{4+}}$ stands for the effect of the CaO-MnO binary on the activity of Si^{4+}. Expressions for the partial excess Gibbs energies and the effects from the other binaries are given in Table 1. The Gibbs energy of fusion for MnO is presented in Table 2.

The MnO activities in this ternary at 1923 K were measured by Abraham *et al.* /29/ as well as Mehta and Richardson /30/ by equilibrating slags with Pt-Mn alloys. The results of the two experimental studies differ somewhat from each other. A comparison between experimental values and the calculated iso-activity lines is presented in Figure 7a. While the results of model calculations compare well with the experimental values by Mehta and Richardson, the values reported by Abraham *et al.* /29/ differ from both the present calculation and the results of Mehta and Richardson /30/. Iso-activity lines of CaO are presented in Figure 7b

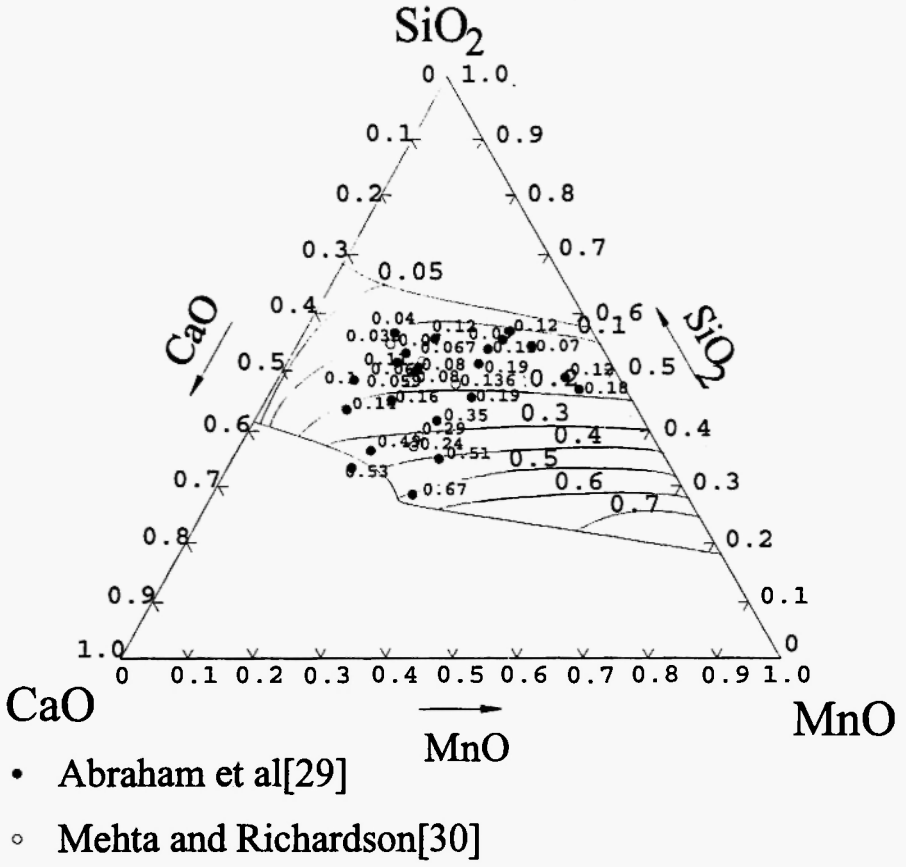

Fig. 7a: Experimental values of the activities of MnO from Abraham *et al.* /29/ and Mehta and Richardson /30/ at 1923 K compared with the calculated iso activity lines at the same temperature. The standard state is pure solid MnO.

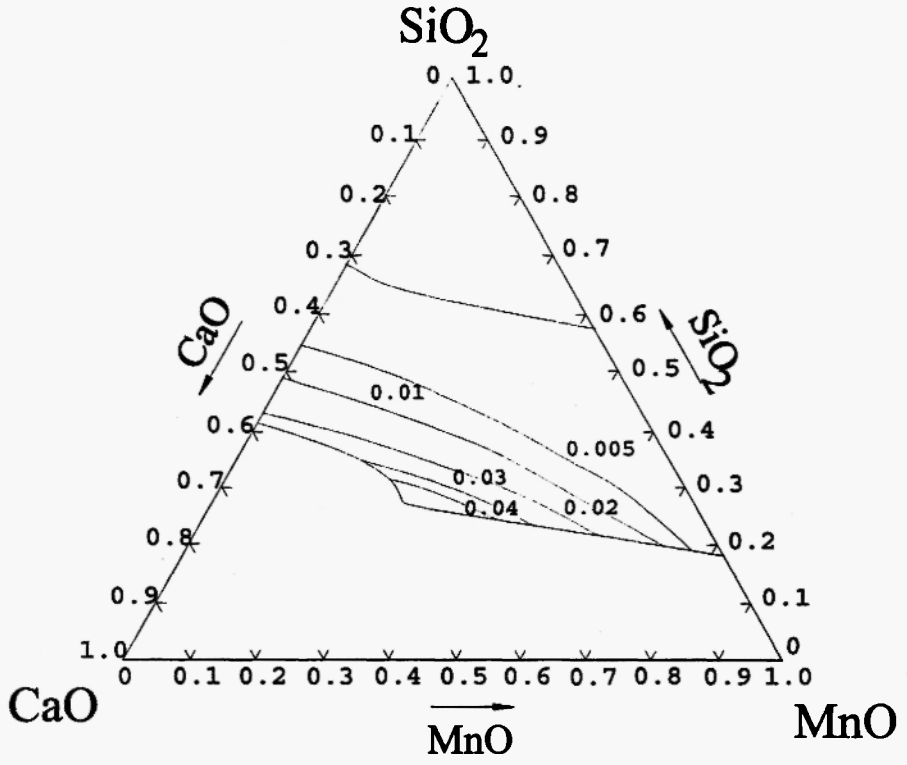

Fig. 7b: Iso activity lines of CaO in the CaO-'MnO'- SiO_2 system at 1923 K calculated by the model. The standard state is pure solid CaO.

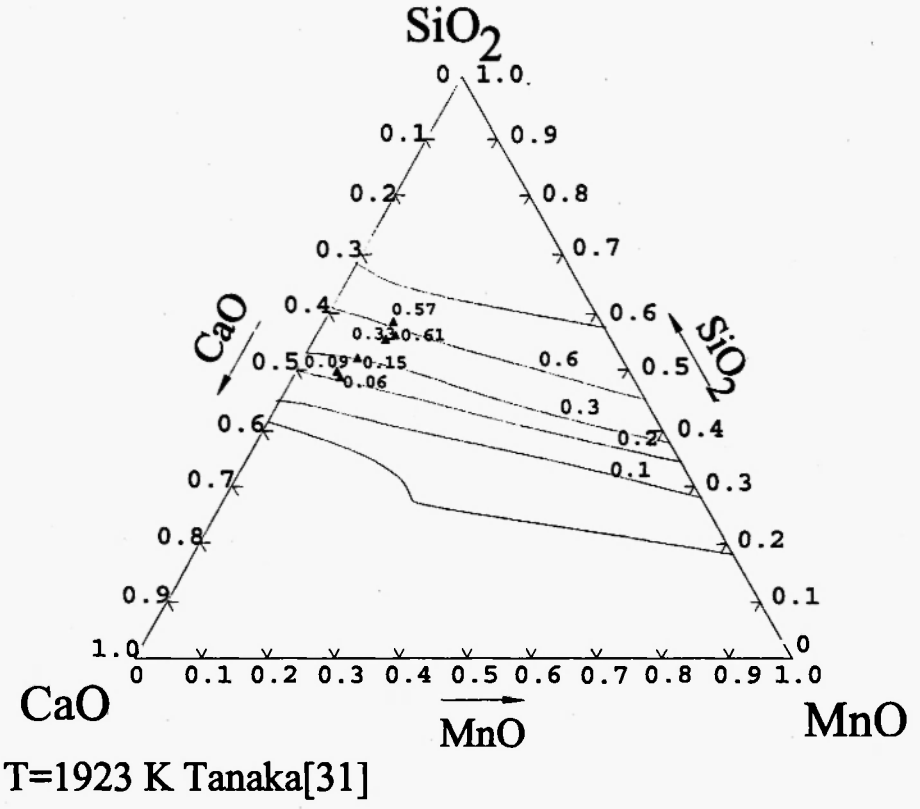

Fig. 7c: Experimental values of activities of SiO_2 from Tanaka /31/ at 1823 K and calculated iso activity lines at 1823 K. The standard state is pure solid SiO_2.

at 1923 K. Tanaka /31/ measured the activities of SiO_2 at 1773 K and 1823 K using the equilibrium between Mn-Si-C_{sat} liquid alloys and slags. His activity values are plotted in Figure 7c along with the iso-activity lines of SiO_2 at 1823 K. The agreement with the model is not good except in the region of high SiO_2 activities. Sawamura /9/ carried out measurements of CaO activities using the EMF technique similar to the method adopted for the CaO-SiO_2 system described earlier. Their experimental values at 1873 K are compared with the calculated activities in Figure 8.

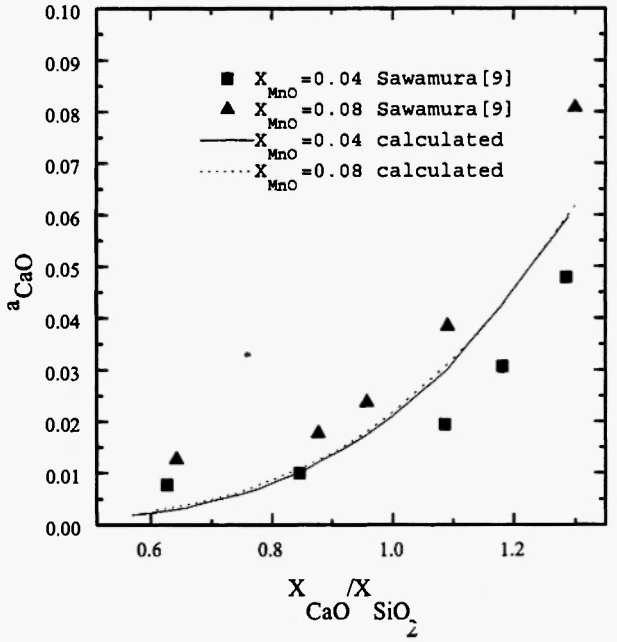

Fig. 8: Calculated and experimentally determined /9/ activities of CaO in the CaO-'FeO'- SiO_2 system at 1873 K. The standard state is pure solid CaO.

3. DISCUSSION

The agreement between the results of model calculation and the experimental data for the systems CaO-SiO_2, CaO-'FeO', 'FeO'-SiO_2 /7/ and MnO-SiO_2 /7/ demonstrates the reliability of the present model in extrapolating and interpolating the experimental data in the case of binary slag systems. In the case of ternary systems CaO-'FeO'-SiO_2 and CaO-MnO-SiO_2, the agreement between the model predictions in the present work and the experimental data available in the literature can generally be considered satisfactory. However, it should be mentioned that the activities of SiO_2 calculated by the model differ from the only available experimental data in the literature reported by Tanaka /31/ on the CaO-MnO-SiO_2 system. This difference could be due either to possible inadequacies of model calculation or the uncertainties involved in the experiments. There is a possibility that the assumption $\Omega^{FeCa(O)} = \Omega^{CaFe(O)}$ might introduce some uncertainties in the model calculations. But the agreement between the model predictions and the experimental data in the case of both CaO activity and MnO activity does not seem to suggest that that is the case. It is difficult to clarify the reason at the present stage, since there is no other source of the experimental data for the SiO_2 activities, which emphasises the need for further experimentation. Despite this uncertainty in the SiO_2 activity, the overall agreement between the model predictions and the experimental results in the ternary systems indicates that the slag model can also be used for the ternary silicate systems, where the two basic cations differ in size.

It is seen that CaO shows a significant negative deviation in the CaO-SiO_2 binary, as well as the CaO-'FeO'-SiO_2, and the CaO-MnO-SiO_2 ternary systems. This behavior is in strong contrast to the other basic oxides, 'FeO', MnO and MgO /7/ in silicate melts. This is very important in the case of thermodynamic modelling of metallurgical processes, since any assumption of an ideal solution would lead to great error. The ability of the present model to estimate the oxide activities in ternary silicate slags has shown the great potential of the model in predicting the thermodynamic properties of multicomponent slags.

Calculations have been performed in the quaternary system CaO-'FeO'-MnO-SiO_2. The expression for the integral excess Gibbs energy for the CaO-'FeO'-MnO-SiO_2 liquid phase can be expressed as:

$$G^E = y_{Ca}y_{Fe}\Omega^{CaFe(O)} + y_{Ca}y_{Mn}\Omega^{CaMn(O)} + y_{Ca}y_{Si}\Omega^{CaSi(O)} + y_{Fe}y_{Si}\Omega^{FeSi(O)} + y_{Fe}y_{Mn}\Omega^{FeMn(O)} + y_{Mn}y_{Si}\Omega^{MnSi(O)} \quad (17)$$

This expression can be used to derive the partial excess Gibbs energies for the respective oxides:

$$G_i^E = G^E + \frac{\partial G^E}{y_i} - \sum y_i \frac{\partial G^E}{y_i} \quad (18)$$

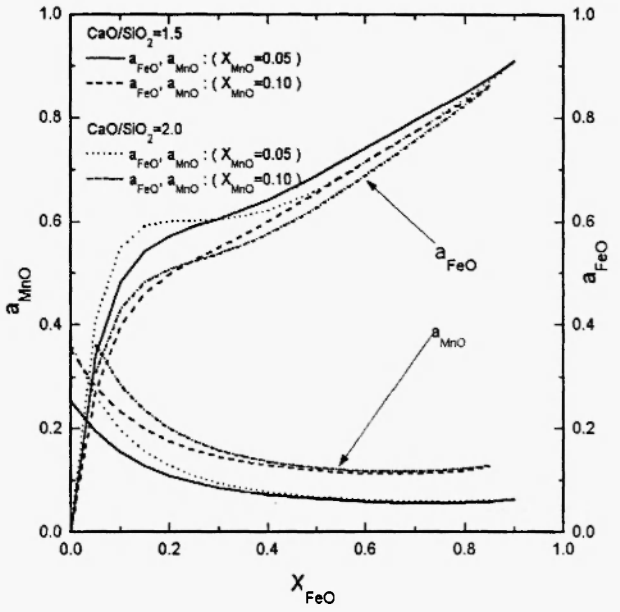

Fig. 9: Calculated activities of 'FeO'-and MnO in the system CaO-'FeO'-MnO-SiO_2 at constant mole fractions of MnO (x_{MnO} = 0.05 and x_{MnO} = 0.10) and 1873 K. The standard states are pure liquid 'FeO' and pure solid MnO.

No experimental determination of steel making temperatures is available in the literature. In Figure 9, the 'FeO' and MnO activities are plotted against the mole fraction of 'FeO' at constant MnO contents and constant ratio between CaO and SiO_2 at 1873 K. From the figure, it is seen that an increase in MnO concentration gives a rapid decrease in the 'FeO' activity in the region of low 'FeO' contents. When the CaO concentration decreases, both the 'FeO' and MnO activities will increase in the region of low 'FeO' contents. This system is important in the normal low alloy steel converter. The 'FeO' activity at constant MnO mole fraction (x_{MnO} = 0.05) at 1873 K is presented in Figure 10. Comparison of Figure 6a and Figure 10 shows that the addition of MnO to CaO-'FeO'-SiO_2 melts decreases the 'FeO' activity. This would lower the slag's ability to re-oxidize the hot metal in the converter process.

The model could be used in converter models to evaluate the equilibrium conditions. However, since alumina is another important component in metallurgical slags, the application of the present model to industrial slags necessitates consideration of this oxide.

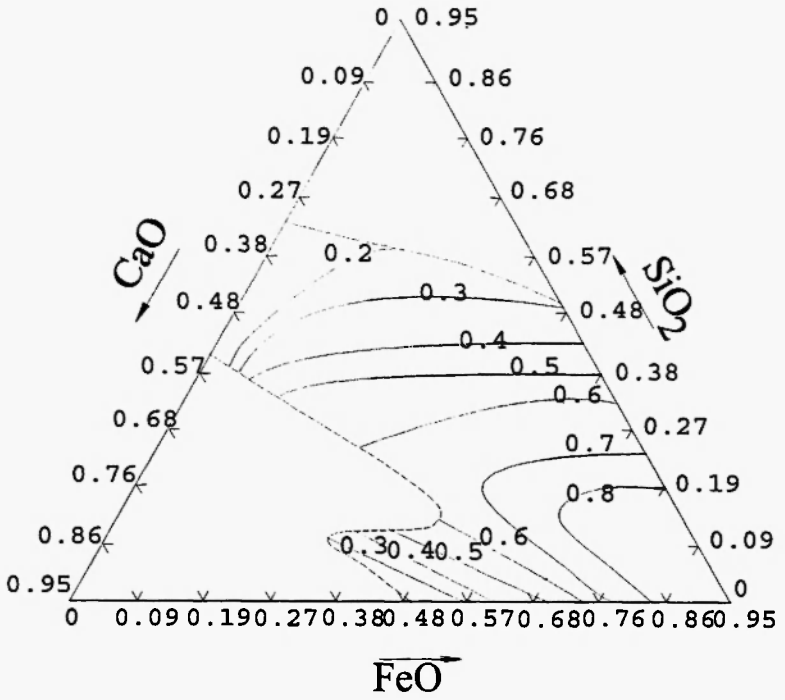

Fig. 10: Iso activity lines of 'FeO' in the system CaO- 'FeO'-MnO-SiO_2 with a constant mole fraction of MnO (x_{MnO} = 0.05). The standard state is pure liquid 'FeO'.

In order to establish a platform for the use of the model in processing modelling and controlling, it is necessary to examine the applicability of the model to the melts containing Al_2O_3 that is amphoteric in nature. Both experimental and modelling studies are currently being carried out in the present laboratory to investigate this aspect.

4. SUMMARY

The oxide activities in the CaO-SiO_2 and CaO-'FeO' binary as well as the CaO-'FeO'-SiO_2 and CaO-MnO-SiO_2 ternary melts have been calculated using a slag model developed in the present laboratory. Based on the assessed experimental data for the CaO-SiO_2 and CaO-'FeO' systems, model parameters describing the $Ca^{2+}Si^{4+}$ and Ca^{2+}-Fe^{2+} interactions in the presence of oxygen ions have been obtained. The good agreement between the results of model calculations and the experimental data for the systems CaO-SiO_2 and CaO-'FeO' has demonstrated the reliability of the slag model in extrapolating and interpolating the experimental data in binary systems. Expressions to predict oxide activities in the two ternary systems, CaO-'FeO'-SiO_2 and CaO-MnO-SiO_2 using only the binary parameters based on binary experimental information have been suggested. The agreement between the model predictions and the experimental results in the ternary systems has further indicated that the slag model can be employed for ternary silicate systems, where the two basic cations have a great difference in size.

REFERENCES

1. C.F. Manson. Thermodynamics and constitution of silicate slags, in: *Int. Symp. Metallurgical Chemistry – Applications in Ferrous Metallurgy*, Iron & Steel Inst., 1971; 3-11.
2. M. Hillert, B. Jansson, B. Sundman and J. Ågren. *Metall. Trans.*, **16A**, 261-266 (1985).
3. H. Gaye and J. Welfringer. *Second Int. Symp., Metallurgical Slag and Fluxes*, Nevada, 1984; 357-375.
4. J. Lumsden. *Int. Symp., Physical Chemistry of Process Metallurgy*, Part 1, AIME, 1959; 165-205.
5. M. Temkin. *Acta Phys. Chim. U.R.S.S.*, 20(4), 411-420 (1945).
6. J. Bygdén, Du Sichen and S. Seetharaman. *Steel Research*, **10**, 421-428 (1994).
7. J. Björkvall. Du Sichen and S. Seetharaman. Submitted for publication to *High Temp. Mater. & Proc.*, 1999.
8. F.D. Richardson. *Trans. Faraday Soc.*, **52**, 1312-1224 (1956).
9. K. Sawamura. *Tetsu-to-Hagane* (Overseas), **2**, 219-225 (1962).
10. K. Sanbongi and Y. Omori. *Physical Chemistry of Metallic Solutions and Intermetallic Compounds, II, Section 6, 6d*, London, 1959; 1-10.
11. Y. Omoni and K. Sanbongi. *J. Metals Inst. Japan*, **25**, 139-143 (1961).
12. V.L. Stolyarova, S.I. Shornikov, G.G. Ivanov and M.M. Shultz. *J. Electrochem. Soc.*, **138**, 3710-3714 (1991).
13. H.R. Rein and J. Chipman, *Trans. Metallurg. SOC AIME*, **233**, 415-425 (1965).
14. P.T. Carter and T. Macfarlane. *J. Iron Steel Inst.*, **185**, 54-66 (1957).
15. R.A. Sharma and F.D. Richardson. *J. Iron Steel Inst.*, **200**, 373-379 (1957).
16. D.A.R. Kay and C.R. Taylor. *J. Trans. Faraday Soc.*, **56**, 1372-1386 (1960).
17. J.C. Fulton and J. Chipman. *Trans. Metallurg. Soc. AIME*, **200**, 1136-1146 (1954).
18. *Slag Atlas*, 2nd ed., Verein Deutscher Eisenhüttenleute ed., Verlag Stahleisen GmbH, D-Düsseldorf, Germany, 1995; 142.
19. S. Ban-Ya, A. Chiba and A. Hikosaka. *Tetsu-to-Hagane*, **66** (10), 1484-1493 (1980).
20. Y. Takeda and A. Yazawa. *Nippon Kogyokaishi*, 96, 901-906 (1980).
21. M. Iwase, N. Yamada, K. Nishida and E. Ichise. *Trans. Iron Steel Soc. AIME*, **4**, 69-75 (1984).
22. M. van Wijngaarden and R. Dippenaar. *J. S. Afr. Inst. Min. Metall.*, **86** (11), 443-453 (1986).
23. H. Fujita, Y. Iritani and S. Maruhashi. *Tetsu-to-Hagane*, **54**, 359-370 (1968).
24. C.R. Taylor and J. Chipman. *Trans. AIME*, **154**, 225-247 (1954).
25. C. Bodsworth. *J. Iron Steel Inst.*, **193**, 13-24

(1959).

26. Y. Wanibe, Y. Yamauchi, K. Kawai and H. Sakao. *Arch. Eisenhuttenwes.*, **44** (9), 711-717 (1973).
27. M. Timucin and A.E. Morris. *Metall. Trans.*, **1**, 3193-3201 (1970).
28. T. Ogura, R. Fujiwara, R. Mochizuki, Y. Kawamoto, T. Oishi and M. Iwase. *Trans. Metall.*, **23B**, 459-466 (1992).
29. K.P. Abraham, M.W. Davies and F.D. Richardson. *J. Iron Steel Inst.*, **196**, 82-89 (1960).
30. S.R. Mehta and F.D. Richardson. *J. Iron Steel Inst.*, **203**, 524-528 (1965).
31. A. Tanake. *Tetsu-to-Hagane*, **66** (10), 1474-1483 (1980).
32. I. Barin, F. Sauert, E. Schultze-Rhonhof and W. Shu Sheng. *Thermochemical Data of Pure Substances*, Second Edition, VCH Verlagsgesellschaft mbH, Weinheim, Germany, 1993.